The variation of turbulent burning rate of methane, methanol and iso-octane air mixtures with equivalence ratio at elevated pressure

M. Lawes, M.P. Ormsby, C.G.W. Sheppard and R. Woolley

School of Mechanical Engineering, University of Leeds, Leeds LS2 9JT, UK

Abstract

Turbulent burning velocities for premixed methane, methanol and iso-octane - air mixtures have been experimentally determined for an rms turbulent velocity of 2 m/s and pressure of 0.5 MPa for a wide range of equivalence ratios. Turbulent burning velocity data were derived, using high speed schlieren photography and transient pressure recording; with measurements processed to yield a turbulent mass rate burning velocity, u_{tr}. The consistency between the values derived using the two techniques, for all fuels for both fuel lean and rich mixtures, was good. Laminar burning measurements were made at the same pressure, temperature and equivalence ratios as the turbulent cases and laminar burning velocities and Markstein numbers determined. The equivalence ratio (ϕ) for peak turbulent burning velocity proved not always coincident with that for laminar burning velocity for the same fuel; for iso-octane the turbulent burning velocity unexpectedly remained high over the range $\phi = 1$ to $\phi = 2$. The ratio of turbulent to laminar burning velocity proved remarkably high for very rich iso-octane-air and lean methane-air mixtures.

Introduction

The aim of the experimental study reported here was to examine the influence of equivalence ratio on the turbulent burning velocities of three fuel-air mixtures; methane, methanol and iso-octane. The range of equivalence ratio studied extended to quite rich mixtures (up to $\phi = 2$), reflecting current interest in (for example) gasoline direct injection (GDI) engines. Methane and methanol are widely used in industrial and commercial applications as well as, increasingly, to fuel transport engines. Iso-octane is a commonly adopted representative reference single component fuel having physical and burning properties resembling fuels such as gasoline. The experiments were conducted at a fixed rms turbulent velocity, $u' = 2$ *m/s*, characteristic of the turbulence level encountered in a number of industrial and engine applications (where flames are typically within the wrinkled laminar flame regime (Abraham et al., 1985)). Measurements were performed at an elevated pressure 0.5 *MPa*, where

experimental data are relatively sparse, since this has been shown to result in significant change in laminar flame properties cf. atmospheric combustion. These properties include reduction of the laminar burning velocity, u_l, flame thickness, δ_l and Markstein number (Bradley et al., 1998; Gu et al., 2000).

In this study, burn rate has been characterised by a turbulent burning velocity. Recent work has shown the importance of unambiguous definition of this parameter, and the flame surface area associated with it (Lipatnikov and Chomiak, 2002; Gillespie et al., 2000; Bradley et al., 2003). Two turbulent burning velocities are most commonly used: (i) the velocity of entrainment of fresh unburned gas into the flame, u_{te}, associated with a mean surface area representing the leading edge of the flame and (ii) a velocity, u_{tr}, representing the mass rate of burning necessary to produce the actual rate of heat release, associated with a smooth mean surface area separating burned from unburned gas. These two burning velocities are not identical, because of unburned gas existing behind the leading edge of the turbulent flame and the different flame surface area definitions. Flame propagation monitored using ciné photography generally yields a parameter directly related to u_{te} , whereas pressure records (in conjunction with 2-zone combustion models) yield values for u_{tr} (Lewis and von Elbe, 1984). Employing the same vessel as that used in the currently reported study, recent simultaneous ciné schlieren and laser sheet imaging experiments of propane – air flames (for u'/u_l up to 10.7 (Bradley et al., 2003)) has provided a means for deriving u_{tr} from flame radii generated from schlieren imaging via the empirical expression:

$$u_{tr} = \left(0.9\,\rho_b/\rho_u\right) dR_{sch}/dt \qquad (1)$$

where ρ_u and ρ_b are the unburned and burned gas densities and R_{sch} is the mean flame radius derived from schlieren images.

Spherically expanding laminar flames, of identical initial pressure and temperature, were monitored at each equivalence ratio and the resulting images processed to provide comparative data for unstretched laminar burning velocity (Bradley et al., 1998).

Experimental

Experiments were performed in a stainless steel vessel of inner diameter 380 mm in which mixtures could be ignited at initial temperatures up to 600 K and initial pressures up to 0.15 MPa. Three orthogonal pairs of quartz windows of 150 mm diameter could be fitted, providing exceptional optical access for imaging and optical diagnostic techniques. Turbulence was generated in the bomb by four identical eight bladed fans situated inside the vessel in a regular tetrahedron configuration (Gillespie et al., 2000). The fans were directly coupled to electric motors with separate speed controllers, each fan was adjustable between 3.3 to 167 Hz.

Within the central region accessible to laser doppler anemometry, it has been established that the fans generated uniform isotropic turbulence; with the rms turbulent velocity proportional to the fan speed. The integral length scale, L, was found (by two-point correlation) to be 20 mm (Nwagwe et al., 2000).

The mixture temperature was measured using a K type thermocouple situated inside the vessel. The entire vessel was preheated by a 2 KW heater situated in the vessel. In this study the initial mixture temperature was set to 360 K, this ensured complete evaporation of the liquid fuels and avoided excessive condensation on the wall after an ignition. An absolute pressure transducer was employed to measure the initial mixture pressure, this transducer was situated outside the vessel and was isolated just prior to ignition. Mixtures were prepared in the vessel, which was initially evacuated. In the cases of methanol and iso-octane, the required quantity of fuel was injected in the liquid state - using a calibrated syringe. In the case of methane, the fuel was supplied from a pressurised cylinder and the mixture prepared on the basis of partial pressures. For all fuels dry air was added from a cylinder to make up the mixture to the required pressure at ignition. The desired temperature was achieved by preheating the whole vessel to the required temperature. Running the fans resulted in the fresh mixture being rapidly heated to the vessel temperature and ensured complete mixing of the fuel and air. Ignition was initiated using a sparkplug mounted in the centre of the vessel. A Lucas 12 V transistorised automotive ignition coil system was connected to the sparkplug. The ignition circuit was earthed via the main body of the vessel. Average spark energy supplied to the plug was measured to be 23 mJ.

The history of pressure development in each deflagration was monitored with a Kistler 701 pressure transducer, flush mounted on the side of the vessel. To maximise accuracy of pressure measurement in the early stages of the flame progress, the sensitivity of the charge amplifier was set such that the full range of the 12 bit analogue to digital converter was used to capture the first 0.1 MPa pressure rise. The analysis procedures of Lewis and von Elbe (1984) were adopted for processing the resulting pressure traces to yield burning velocities.

High speed schlieren images of combustion events were captured using one of two digital cameras. For the majority of the experiments a Photosonics Phantom 4 high speed camera was adopted; an alternative Kodak HS 4540 camera was used in some early tests. A helium-neon laser light source used in the early experiments was later replaced with a 20 W tungsten element lamp; giving significant improvement in image quality. The laminar flames were captured at 1000 fps over 512x512 pixels. Turbulent flames were recorded at 3700 fps (4500 fps with the Kodak HS 4540) over 256x256 pixels. Five turbulent deflagrations were recorded at each condition. The flame area was found by converting each grey scale image to a binary (black and white) image, corresponding to unburned and burned gas. This operation was performed as a semi automated batch process within Adobe Photoshop. The area was then found by counting the number of white (burned) cells. Mean flame radius was determined as that of a circle encompassing the same area.

With all fuels, the images of the leanest turbulent (and rich methane-air) flames exhibited evidence of flame extinction, with parts of the schlieren edge becoming less distinct with time. This resulted in difficulties in image processing and inconsistent development of derived flame radius and burning velocity from one frame to the next. The stoichiometric and fuel rich (iso-octane and methanol) flames produced a clearly defined consistent edge.

Results and Discussion

Shown in Fig. 1 are schlieren images of 4 turbulent flames at radii of 5, 10, 20 and 30 mm. The first three columns show developing methane-air flames at ϕ = 0.6, 1.0 and 1.3. The final column is for an iso-octane – air flame at ϕ = 1.8. The methane ϕ = 0.6 sequence has been selected to illustrate a particularly extreme example of a flame that is convected away from the point of ignition. Although part of the flame does stay around the spark plug, the main flame is ripped from, and starts growing away from, the igniter. As schlieren photography

produces an image integrated in the third dimension, it is impossible to know whether the two 'kernels' are actually connected, as they seem on the image. The growth of this particular flame may well not be properly represented by successive radii of equivalent spherical flames. The ϕ = 1.0 and 1.3 flame sequences can be seen to be very similar and were typical of most of the flames observed, the kernels remaining around the spark plug and the flames growing relatively, if not perfectly, symmetrically. In contrast, the rich iso-octane – air flame growth can be seen to be remarkably circular and to have a strong well defined flame edge.

Shown in Fig. 2(a) (symbols) are typical schlieren image derived mean flame radius and pressure histories, plotted against time from ignition for three selected equivalence ratios for, in this case, methane flames. Corresponding values of u_{tr} , derived from successive schlieren images and application of Eq.1, are displayed in Fig.2(b). Note that it was only possible to process image data for turbulent flames to a mean (equivalent spherical) reaction surface radius of 50-60mm; beyond this, as a result of flame kernel centroid migration, flame shape distortion and turbulent flame brush thickness, some part of the flame circumference would extend beyond the viewing area (window radius = 75 mm). Note also, Fig. 2(a), that during this flame development period, there was very little pressure and associated temperature rise – they remained essentially constant at their set initial values. Hence it was only possible to derive meaningful values of pressure derived u_{tr} for a relatively narrow range of mean flame radii/times elapsed from ignition, Fig. 2(b). At earlier flame radii the pressure rise was too low relative to signal noise for accurate determination of u_{tr}, at greater radii the flame grew beyond the central region of defined turbulence characterisation, into fan interference and significantly rising unburned gas pressure and temperature. High frequency oscillations are evident on a number of the pressure derived burning velocities; they are thought most likely to be due to the relatively low pressure signals resulting in experimental noise, although it is not impossible that they could be combustion generated. The region of overlap in meaningful values of u_{tr} derived using the two techniques was relatively small. Nevertheless, the agreement seen in Fig. 2(b) (typical for the range of fuels and conditions examined) was gratifying and engendered a degree of confidence in the experimental methods and analysis techniques.

Schlieren image derived mean flame radius, pressure histories and u_{tr} values are shown for three methanol and iso-octane flames in Figs. 3 and 4. For each fuel representative

stoichiometric and extreme fuel lean and rich flames were selected. The agreement between the schlieren and pressure derived values of u_{tr} can again be seen to be remarkably good.

After the initial spark disturbance, all the flames represented in Figs. 2(b), 3(b) and 4(b) can be seen to have accelerated continuously, although at different rates for different fuels and equivalence ratios. This was primarily associated with turbulent flame development. Immediately after ignition, a flame kernel is essentially laminar and is initially wrinkled by only the smallest eddies within the turbulent spectrum; as the flame grows, more of the turbulent spectrum becomes available to wrinkle the flame surface (Abdel-Gayed et al., 1987).

To effect comparison of magnitude and behaviour pattern with equivalence ratio for the three fuels, values of schlieren derived u_{tr} were found for flames at a mean flame radii of 10 and 30 mm, Fig. 5. At a given mean flame radius (kernel size), on the average, the scales of turbulence within the spectrum able to influence the growing flame will be equal in each case (Abdel-Gayed et al., 1987); here, the corresponding values of effective turbulence 'intensity', u_k', at these radii were 0.9 and 1.27 m/s. At both radii, considerable scatter in the results for the 5 individual deflagrations at each condition is evident in Fig. 5; this shot to shot 'cyclic variation' is to be expected for a stochastic turbulent environment. A third order least square curve fitting routine was used to generate the curves through each set of experimental data. The standard deviation from the fits was found to be 0.1 m/s at 10 mm and 0.13 m/s at 30 mm; fuel type had no influence. The same overall trends were observed at both these (and other) radii, although the burning velocities at 30 mm were higher than those at 10 mm, as expected with greater turbulent flame development. For all three fuels, the curve fits to the data can be seen to be 'bell-shaped', with u_{tr} values peaking at some equivalence ratio and falling away as the mixtures became leaner and richer, Fig. 5. For methane, the turbulent burning velocity peaked at around $\phi = 0.9$ and then fell away symmetrically as the equivalence ratio increased and decreased. For methanol, the peak occurred at $\phi = 1.25$; as the mixtures became leaner u_{tr} decreased slightly more rapidly than for the rich mixtures. The burning velocities for methanol were higher than those of methane for $\phi \geq 0.9$. However for leaner mixtures values of u_{tr} for methane were slightly in excess of those for methanol. Iso-octane exhibited generally lower burning velocities than the other fuels, it also yielded the lowest peak value of u_{tr}. This peak also occurred at a somewhat richer equivalence ratio ($\phi = 1.4$) than for the other fuels. As the iso-octane mixtures became leaner, the magnitude of u_{tr} fell.

However on the rich side, the u_{tr} value decreased surprisingly little; particularly at greater mean flame radius.

To aid the interpretation of the turbulent measurements the schlieren flame images for spherically expanding laminar flames were processed to yield unstretched laminar burning velocities, u_l, shown in Fig. 6 (Bradley et al., 1998; Gu et al., 2000). In some cases the flames become unstable, developing a cellular structure and enhanced flame speed (Bradley et al., 2000). However an initial period of stable flame propagation was observed in all cases except for rich iso-octane flames, $\phi > 1.2$, where the flames were cellular from inception. As a result, for iso-octane mixtures of $\phi > 1.2$, there was an estimated over-prediction of 10 % in the determination of u_l; over and above other experimental and processing errors (of order 10 % (Bradley et al., 1998) although the shot to shot variation was generally better than 2.5 % for all laminar conditions). For this reason a dashed line has been used in Fig. 6 for these results. The two slowest burning mixtures (methane-air at $\phi = 0.6$ and iso-octane-air at $\phi = 2.0$) were significantly affected by buoyancy; resulting in non-spherical flames (albeit still expanding with a smooth surface).

For each fuel, the turbulent burning velocity at 30 mm was normalised by the corresponding unstretched laminar burning velocity at the same equivalence ratio; the results are shown in Fig. 7. Over the range $\phi = 1.0$ to 1.3, the magnitude of u_{tr} was approximately 4 times u_l for all the fuels. Away from these equivalence ratios, considerable differences in the behaviour of the fuels can be seen. For methane, the ratio of u_{tr}/u_l can be observed to be above 10 at $\phi = 0.6$; thereafter falling with increase in equivalence ratio, before becoming essentially constant above $\phi = 1.0$. In the case of methanol, the magnitude of u_{tr}/u_l can be seen to remain comparatively constant with equivalence ratio (compared with the other fuels); with $u_{tr}/u_l = 4$ for a stoichiometric mixture rising to about 6 at the extreme fuel rich and lean equivalence ratios. Lean iso-octane can be seen to exhibit the lowest value of u_{tr}/u_l, of 2.5 at $\phi = 0.8$. However, for this fuel the ratio of u_{tr}/u_l rose continuously with equivalence ratio to values exceeding 20 at $\phi = 2.0$.

The data processing required to derive u_l also yielded a Markstein Number (Bradley et al., 1998; Gu et al 2000); the obtained values of Markstein Number, Ma_{sr}, corresponding with the unstretched laminar burning velocities are shown plotted against ϕ in Fig.8. The Markstein

number adopted here, Ma_{sr} (Gillespie et al., 2000), has been shown to be that associated with the strain rate of the laminar mass burning velocity, such that:

$$u_l - u_{nr} \approx L_{sr}\alpha_s \qquad (2)$$

where u_{nr} is the strained laminar burning velocity, L_{sr} is the Markstein length and α_s the strain rate. The Markstein number, $Ma_{sr} = L_{sr}/\delta_l$ where δ_l is the laminar flame thickness. Whilst the values of Ma_{sr} obtained were generally very repeatable, they were difficult to determine for cases where the onset of instabilities occurred soon after the cessation of ignition effects (Bradley et al., 1998). This could result in potentially large errors (± 2 or more) in derived Ma_{sr}. Nevertheless, the trends were very consistent and the three fuels clearly exhibited very different responses to stretch rate. Methane-air mixtures exhibited low (even negative) values of Ma_{sr} for lean mixtures, rising progressively to magnitudes of 6 or more for rich mixtures. In contrast, methanol-air mixtures demonstrated small positive values (of $Ma_{sr} \sim 3$) for the leanest mixture – falling to zero or becoming slightly negative as $\phi > 1$, Fig 8. Iso-octane proved to have the most dramatic change in Ma_{sr}, with high positive magnitudes at lean conditions falling sharply to negative values at $\phi = 1.2$. Beyond this equivalence ratio the flames proved cellular from inception and in consequence, although it was possible to estimate values of laminar burning velocity, it was impossible to determine corresponding values of Ma_{sr}. However, it is likely that they were also negative; as flames which are particularly prone to instabilities (such as those noted for the rich iso-octane mixtures) have been associated with negative Markstein numbers (Bradley et al., 2000). The results presented in Fig. 8 are in good qualitative agreement with the calculated Markstein numbers presented by Bechtold and Matalon (2001).

The Markstein Number, Ma_{sr}, expresses the influence of strain rate on laminar flames – with the laminar burning velocity reduced, increased and unaffected for positive, negative and Markstein Number Ma_{sr}, respectively. It has been suggested (Bradley, 2002) that, for a turbulent flame front comprising a series of strained laminar flamelets, the behaviour of u_{tr} would similarly relate to the value of Ma_{sr} for the mixture. The trends in the magnitudes of the ratio u_{tr}/u_l and corresponding values Ma_{sr} for the mixture, Figs 7 and 8, are broadly consistent with this. For methane the highest values of u_{tr}/u_l occurred at the leanest equivalence ratios, where the values of Markstein Number for the mixture were low (of order

zero). Similarly, for iso-octane, the largest values of u_{tr}/u_l also occurred where the mixtures, (in this case at rich) exhibited the lowest (and negative) values of Ma_{sr}. Conversely, methanol, for which (relative to the other two fuels) there was rather less variation of Ma_{sr} with ϕ, exhibited approximately constant behaviour in $u_{tr}/u_{l,}$ with ϕ (cf. the other fuels).

The experimental conditions for each typical turbulent flame is shown plotted on the 'regime' diagram of Peters (2000), Fig. 9, for u' = 2 m/s. Here the laminar flame thickness, δ_l was calculated using ν/u_l, where ν is the kinematic viscosity of the unburned mixture (Peters, 2000). The data shown in this diagram would seem to confirm that the flamelet assumption implied in the previous paragraph was appropriate; it suggests that most of the conditions did indeed fall within the 'corrugated flamelet regime', where a flame is wrinkled by the turbulent eddies and its 'internal' structure is unaffected by the turbulence. However, a few flames are suggested to be within the 'thin reaction zone', where the preheat zone can be disrupted by small turbulent eddies. The flames furthest into the thin reaction were for those mixtures where the value of Ma_{sr} was most likely to have been negative (those of iso-octane – air at ϕ = 1.6, 1.8 , 2.0 and methane-air at ϕ = 0.6).

Laser induced fluorescence images of laminar flames for mixtures exhibiting negative Ma_{sr} have shown that areas of flame front which become concave to the reactants can locally quench, whilst those areas convex to the reactants demonstrate elevated levels of OH radicals (Bradley et al., 2000). It might be argued that the elevated OH is a result of change in the local equivalence ratio associated with differential molecular diffusion; these flame structural effects have been shown to survive into turbulent flames at atmospheric pressure (Haq et al., 2002). The applicability of flamelet concepts to such highly unstable flames, exemplified at these four conditions, might be questionable; as the flame structure appears to be strongly modified by the local flame front geometry, ultimately resulting in areas of quench.

Conclusions

Turbulent and laminar burning velocities of methane, methanol and iso-octane – air mixtures have been measured at a pressure of 0.5 MPa over a wide range of equivalence ratios. The turbulent burning velocity data were derived on the basis of both high speed schlieren photography and transient pressure recording; with measurements processed to yield a

turbulent burning velocity, u_{tr}, characterising the mass rate of burning. The consistency between the values derived using the two techniques, for all fuels for both fuel lean and rich mixtures, proved very good. The values of u_{tr} increased with time and flame radius, as developing flames kernels experienced a greater proportion of the available spectrum of turbulent eddy sizes and energies.

The values of u_{tr} at set mean flame radii were compared with those for laminar burning, u_l, at the measured same initial temperature, pressure and equivalence ratio. For methane and methanol, the trends in variation of turbulent burning velocity with equivalence ratio generally followed those expected on the basis of the behaviour of the laminar burning velocity; although the equivalence ratio yielding the peak value of burning velocity for methane flames was slightly shifted from stoichiometric (or slightly rich of stoichiometric) under laminar conditions to $\phi = 0.9$ in the turbulent case. However, for iso-octane, fuel rich turbulent burning velocities did not follow the trend expected on the basis of laminar burning velocity, remaining high out to quite rich mixtures.

This may have relevance for stratified gasoline direct injection (GDI) engines, where late injection timing is designed to result in locally rich mixture in the vicinity of the spark plug; and have implications for laminar flamelet and other combustion models (which generally do not reflect to noted behaviour).

References

Abdel-Gayed, R.G., Bradley, D., and Lawes, M. (1987) Turbulent burning velocities - a general correlation in terms of straining rates, *Proc. Roy. Soc. Lond.* A, 414, 389-413.

Abraham, J., Williams, F.A. and Bracco, F.V. (1985) *A discussion of turbulent flame structure in premixed charges.* in Engine Combustion Analysis: New Approaches, P-156 also SAE paper 850345.

Bechtold, J.K. and Matalon, M. (2001) The dependence of the Markstein length on stoichiometry. *Combust and. Flame,* 127, 1906-1913.

Bradley, D., Hicks, R.A., Lawes, M., Sheppard, C.G.W. and Woolley, R. (1998) The measurement of laminar burning velocities and Markstein numbers for iso-octane-air and iso-octane-n-heptane-air mixtures at elevated temperatures and pressures in an explosion bomb, *Combust. and Flame***,** 115, 126-144.

Bradley, D., Sheppard, C.G.W., Woolley, R., Greenhalgh, D.A. and Lockett R.D. (2000) The development and structure of flame instabilities and cellularity at low Markstein numbers in explosions, *Combust. and Flame*, 122, 195-209.

Bradley, D. (2002) Problems of predicting turbulent burning rates, *Combust. Theory Modelling*, 6, 361-382.

D. Bradley, D., Haq, M.Z., Hicks, R.A., Kitagawa, T., Sheppard, C.G.W. and Woolley, R. (2003) Turbulent burning velocity, burned gas distribution, and associated flame surface definition, *Combust. Flame*, 133, 415-430.

Gillespie, L., Lawes, M., Sheppard, C.G.W. and Woolley R. (2001) Aspects of laminar and turbulent burning velocity relevant to SI engines, *SAE Trans*. **109**, 13-33 also SAE Technical Paper 2000-01-0192.

Gu, X.J., Haq, M.Z., Lawes, M. and Woolley, R. (2000), Laminar burning velocity and Markstein lengths of methane-air mixtures, *Combust and. Flame*, 121, 41-58.

Lewis, B and von Elbe, G. (1984) *Combustion, Flames and Explosions of Gases*, Third Edition, Academic Press Inc., London.

Haq, M.Z. Sheppard, C.G.W. Woolley, R., Greenhalgh, D.A., and Lockett, R. (2002) Wrinkling and curvature of laminar and turbulent premixed flames, *Combust. Flame*, 131, 1-15.

Lipatnikov, A.N. and Chomiak, J. (2002) Turbulent flame speed and thickness: phenomenology, evaluation, and application in multi-dimensional simulations, *Prog. Energy Combust. Sci*, 28, 1-74.

Nwagwe, I.K., Weller, H., Tabor, G., Gosman, A.D., Lawes, M., Sheppard, C.G.W. and Woolley, R. (2000) Measurements and large eddy simulations of turbulent premixed flame kernel growth, *Proc. Comb. Inst*., 28, 59-65.

Peters, N., (2000) *Turbulent Combustion*, Cambridge University Press, Cambridge, UK.

Methane-air, $\phi = 0.6$ Methane-air, $\phi = 1.0$ Methane-air, $\phi = 1.3$ Iso-octane-air, $\phi = 1.8$

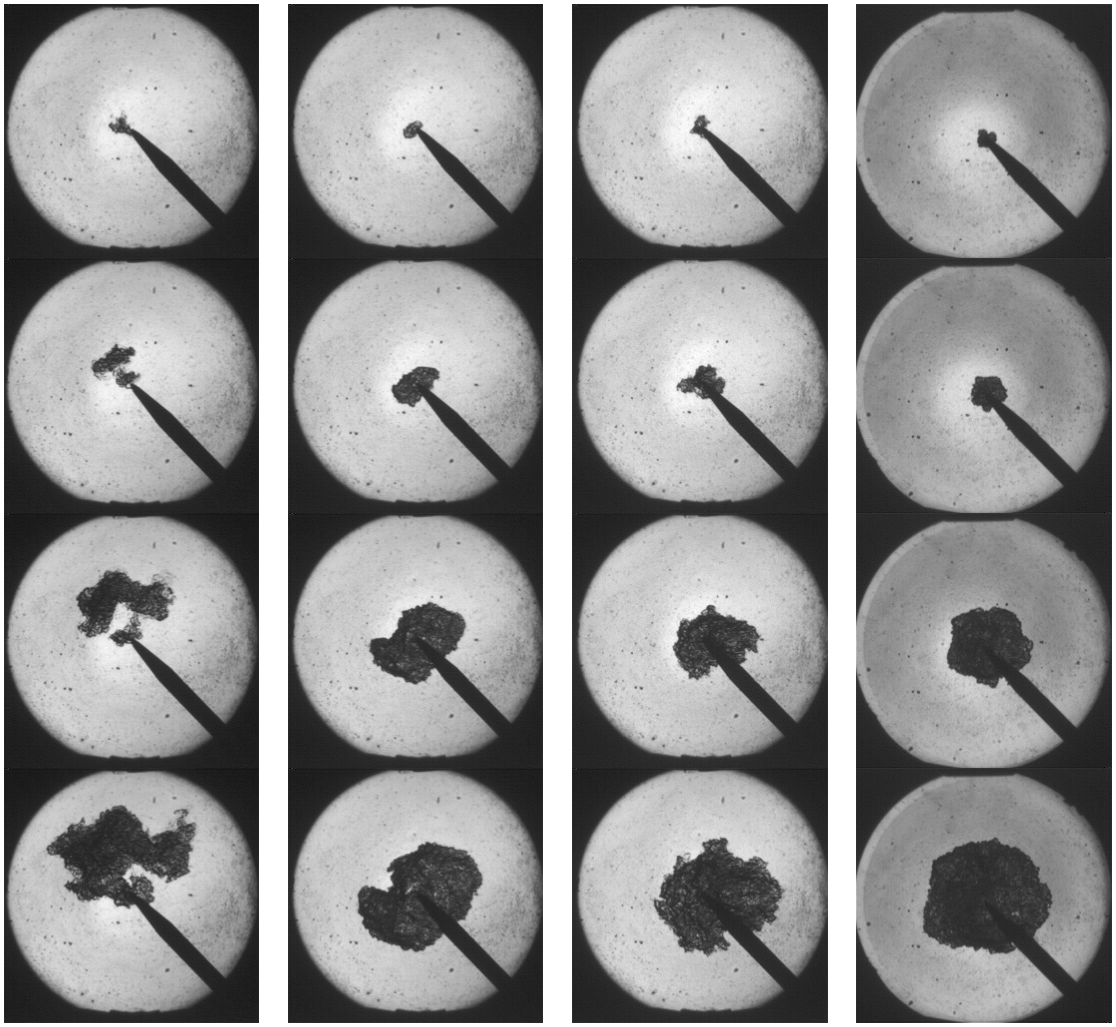

Figure 1. Schlieren images of selected turbulent flames at measured schlieren radii of 5, 10, 20, 30 mm.

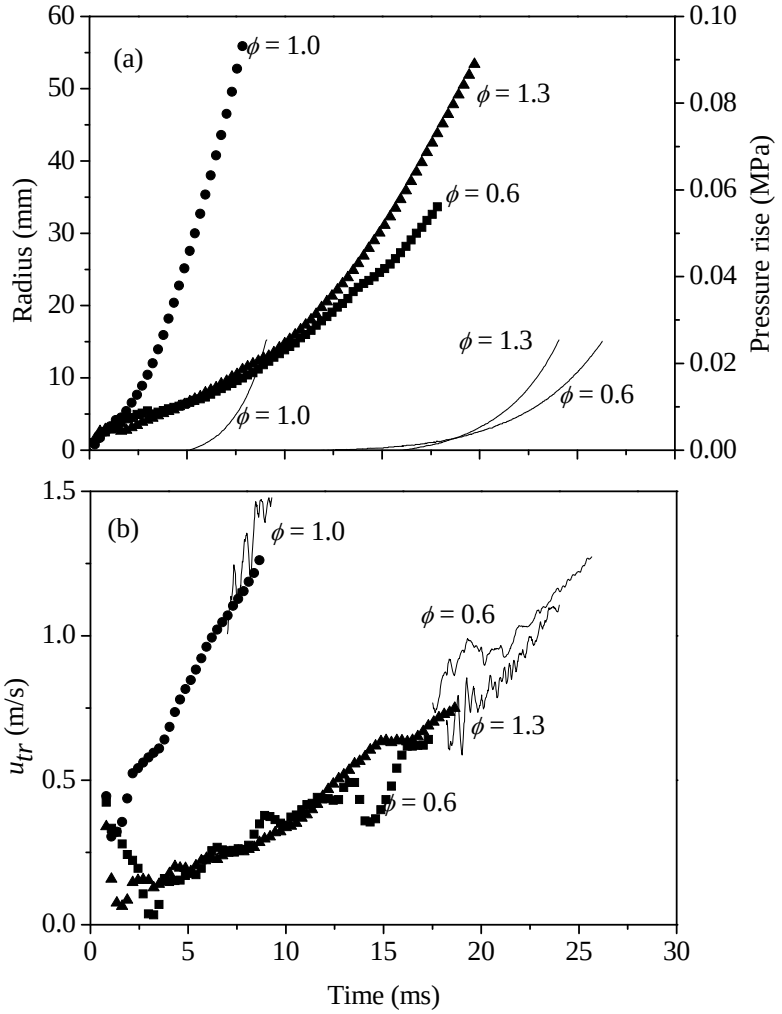

Figure 2. (a) Schlieren flame radius, pressure rise and (b) turbulent burning velocity, u_{tr}, against time from ignition for three methane-air flames at $\phi = 0.6$, 1.0 and 1.3. Symbols derived from schlieren and solid lines from pressure measurements.

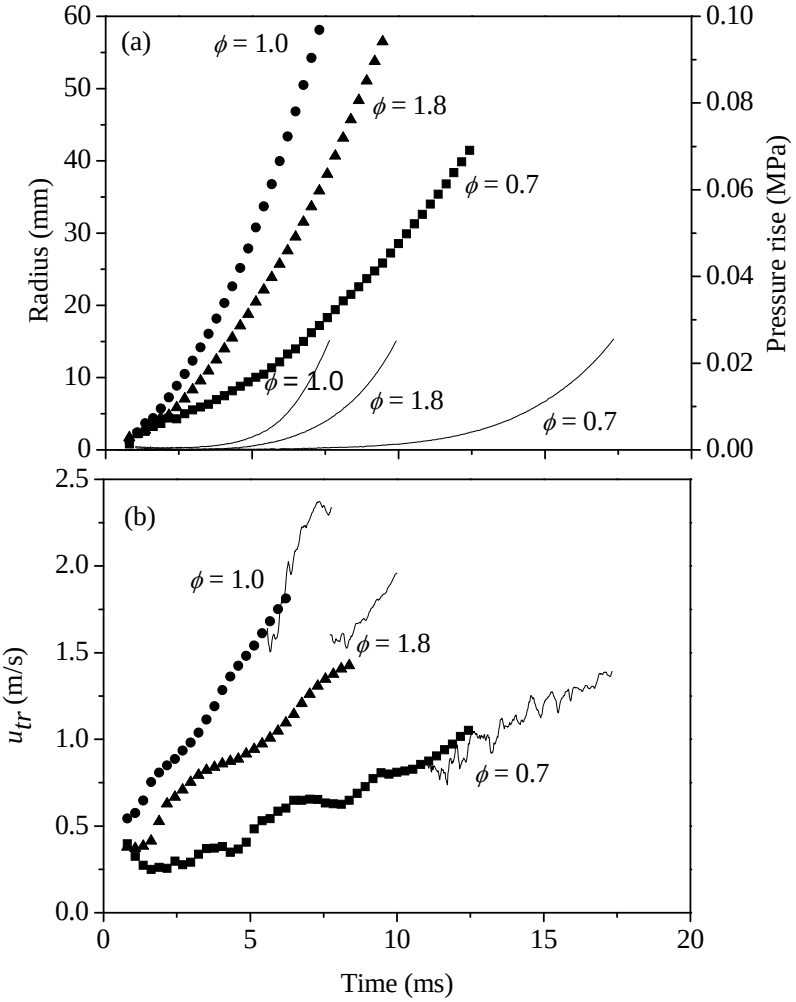

Figure 3. (a) Schlieren flame radius, pressure rise and (b) turbulent burning velocity, u_{tr}, against time from ignition for three methanol-air flames at $\phi = 0.7$, 1.0 and 1.8. Symbols derived from schlieren and solid lines from pressure measurements.

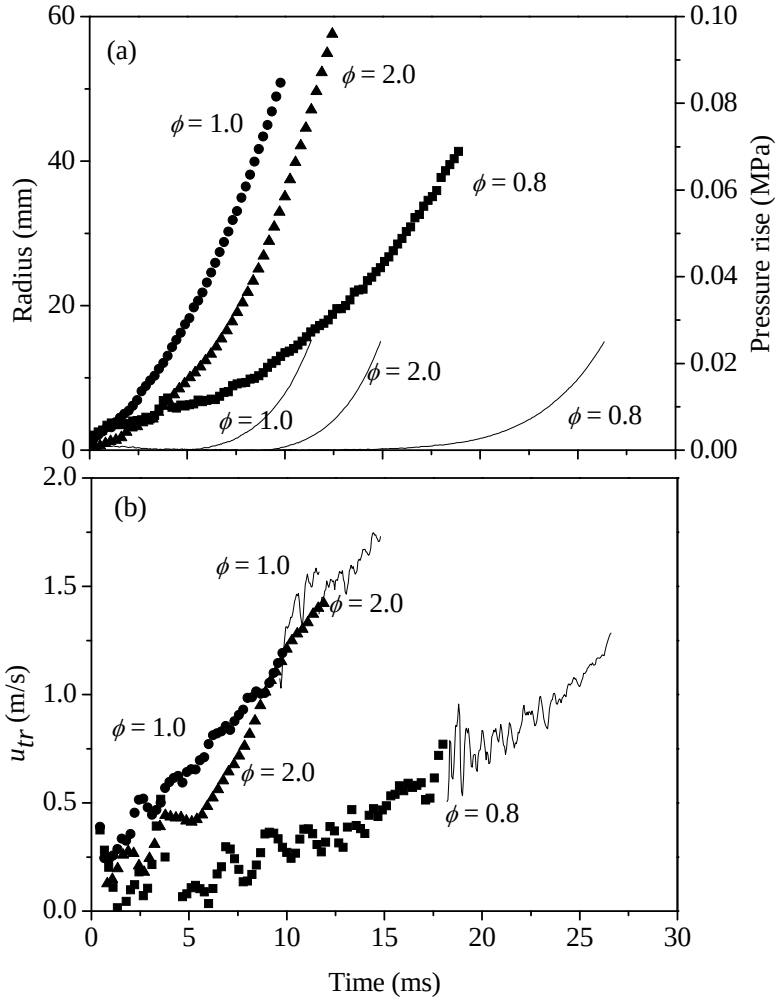

Figure 4. (a) Schlieren flame radius, pressure rise and (b) turbulent burning velocity, u_{tr}, against time from ignition for three iso-octane-air flames at $\phi = 0.8$, 1.0 and 2.0. Symbols derived from schlieren and solid lines from pressure measurements.

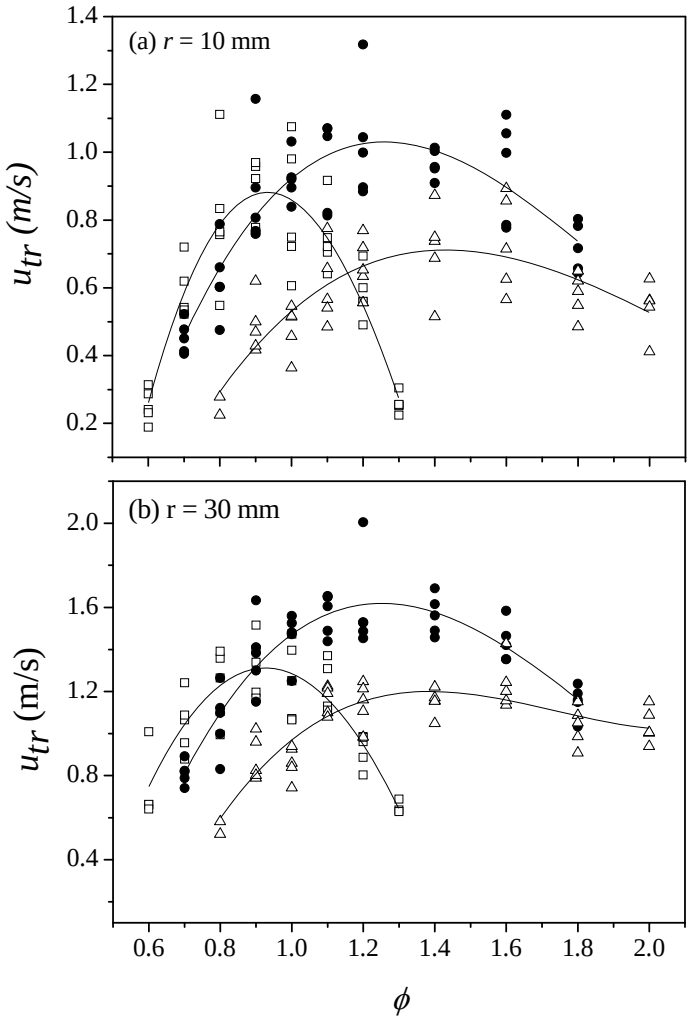

Figure 5. Values of turbulent burning velocity against ϕ at radii of (a) 10 mm and (b) 30 mm. Symbols: squares - methane, circles – methanol, triangles - iso-octane. Lines - third order least square fits.

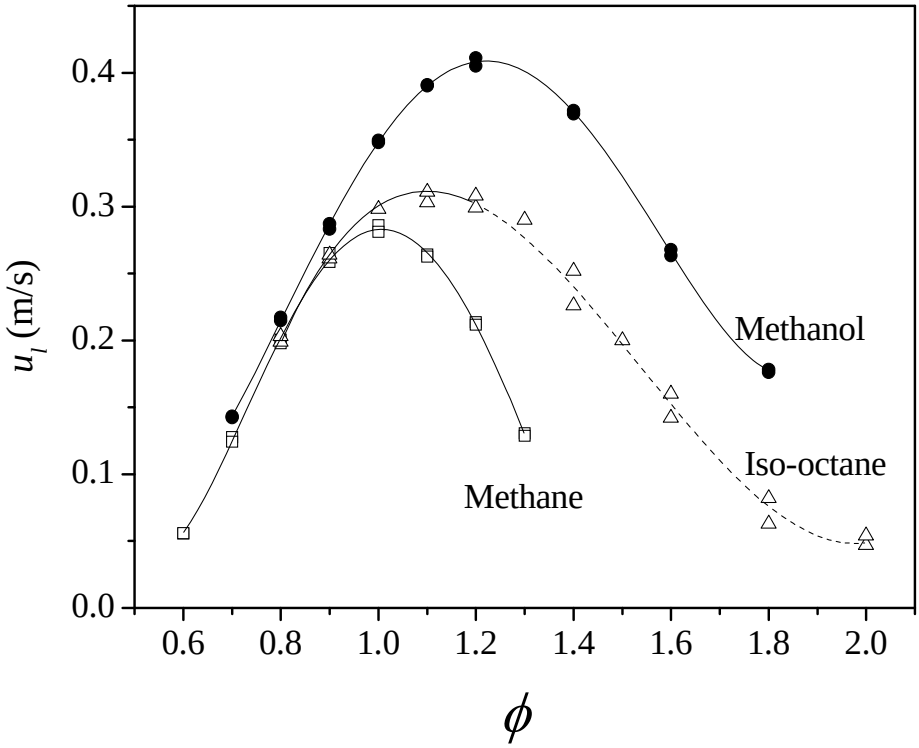

Figure 6. The laminar burning velocity of methane (squares), methanol (circles) and iso-octane – air (triangles) flames against equivalence ratio at 0.5 MPa and 360 K.

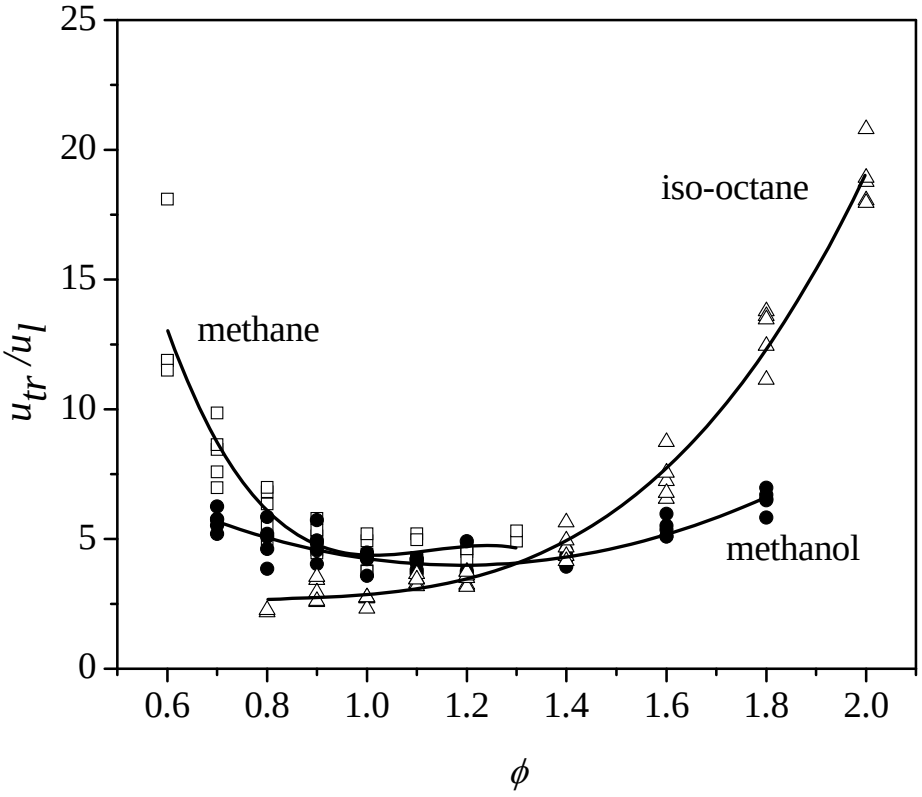

Figure 7. Values of u_{tr}/ul against ϕ for methane (squares), methanol (circles) and iso-octane (triangles). The u_{tr} corresponds to that at a 30 mm flame radius. Lines - least square fits.

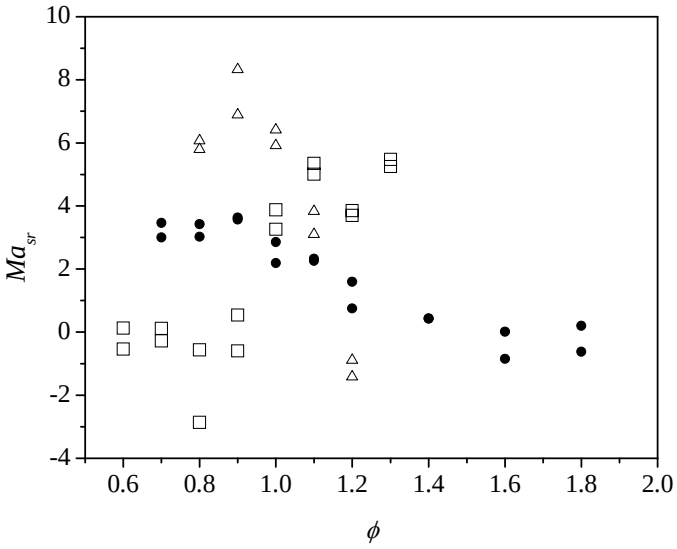

Figure 8. The Markstein number Ma_{sr} of methane (squares), methanol (circles) and iso-octane – air (triangles) flames against equivalence ratio at 0.5 MPa and 360 K.

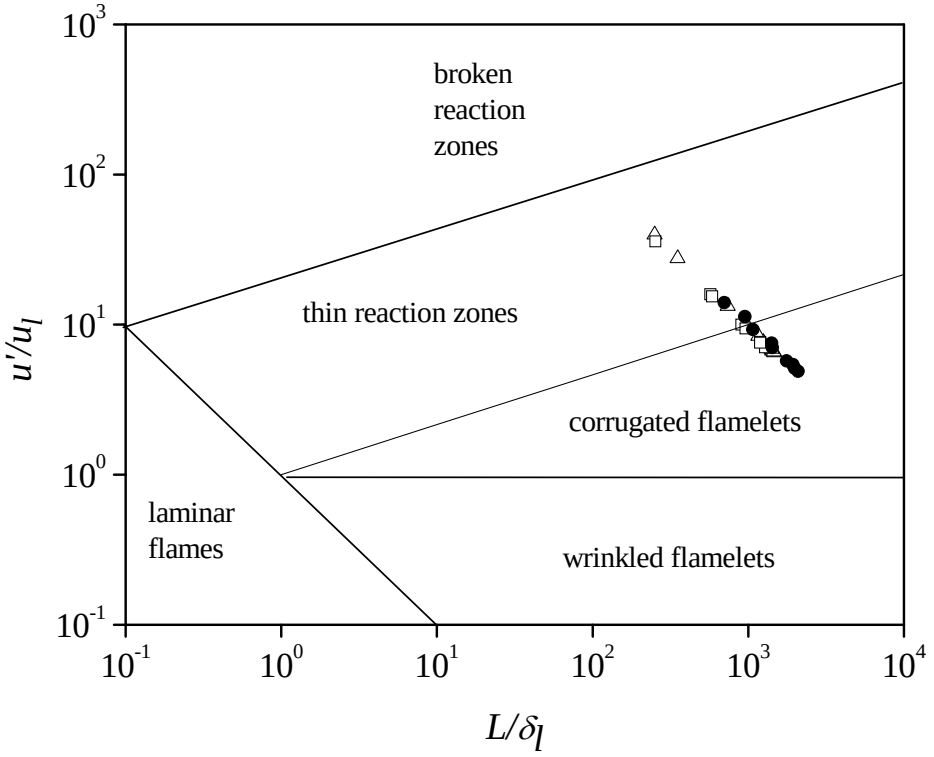

Figure 9. Regime diagram for premixed turbulent combustion. Methane (squares), methanol (circles) and iso-octane – air (triangles).